

Targeting Pro-Tumoral Macrophages in Early Primary and Metastatic Breast Tumors with the CD206-Binding mUNO Peptide

Anni Lepland, Eliana K. Ascitutto, Alessio Malfanti, Lorena Simón-Gracia, Valeria Sidorenko, Maria J. Vicent, Tambet Teesalu,* and Pablo Scodeller*

Cite This: *Mol. Pharmaceutics* 2020, 17, 2518–2531

Read Online

ACCESS |

Metrics & More

Article Recommendations

Supporting Information

ABSTRACT: M2-like tumor-associated macrophages (M2 TAMs) play important roles in the resistance of tumors to immunotherapies. Selective depletion or reprogramming of M2 TAMs may sensitize the nonresponsive tumors for immune-mediated eradication. However, precision delivery of payloads to M2 TAMs, while sparing healthy tissues, has remained an unresolved challenge. Here, we studied the application of a short linear peptide (CSPGAK, “mUNO”) for the delivery of molecular and nanoscale cargoes in M2 TAMs *in vitro* and the relevance of the peptide for *in vivo* targeting of early-stage primary breast tumors and metastatic lung foci. First, we performed *in silico* modeling and found that mUNO interacts with mouse CD206 via a binding site between lectin domains CTLD1 and CTLD2, the same site previously demonstrated to be involved in mUNO binding to human CD206. Second, we showed that cultured M2 macrophages take up fluorescein-labeled (FAM) polymersomes conjugated with mUNO using the sulfhydryl group of its N-terminal cysteine. Pulse/chase studies of FAM-mUNO in M2 macrophages suggested that the peptide avoided lysosomal entrapment and escaped from early endosomes. Third, our *in vivo* studies with FAM-mUNO demonstrated that intraperitoneal administration results in better pharmacokinetics and higher blood bioavailability than can be achieved with intravenous administration. Intraperitoneal FAM-mUNO, but not FAM-control, showed a robust accumulation in M2-skewed macrophages in mouse models of early primary breast tumor and lung metastasis. This targeting was specific, as no uptake was observed in nonmalignant control organs, including the liver, or other cell types in the tumor, including M1 macrophages. Collectively, our studies support the application of the CD206-binding mUNO peptide for delivery of molecular and nanoscale cargoes to M2 macrophages and manifest the relevance of this mode of targeting primary and metastatic breast tumors.

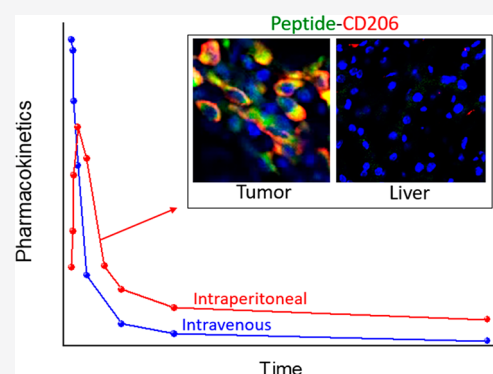
KEYWORDS: tumor-associated macrophages, CD206, immunotherapy, triple-negative breast cancer, homing peptide, pharmacokinetics, nanomedicine, drug delivery systems

INTRODUCTION

Triple-negative breast cancer (TNBC) is the deadliest form of breast cancer.^{1,2} The standard therapeutic approach for TNBC involves combination treatments that are chosen based on stage and other factors, such as age, family history, genetic profile, and personal medical history. Cytotoxic chemotherapy drugs commonly used for TNBC therapy have limited efficacy, and disappointingly, only modest results have been obtained with immunotherapies with checkpoint inhibitors.³ Besides the dense stroma and poor drug penetration,⁴ one of the reasons for the therapeutic failure of immunotherapy of TNBC is that both primary and metastatic TNBC lesions are rich in anti-inflammatory and reparatory M2-skewed macrophages that contribute to these tumors being immunologically “cold” with low infiltration of functional T and natural killer (NK) cells^{5,6} and overexpression of PD-1⁷ and PD-L1.⁸ M2 TAMs also promote metastatic dissemination of TNBC^{9–11} and induce tumor relapse after treatment with taxanes by inducing

secretion of angiogenic factors such as VEGF-A.¹² Due to their central role in tumor progression and therapeutic resistance, M2 TAMs are widely recognized as a translationally relevant target for cancer immunotherapy. Specific affinity targeting of protumoral TAMs may provide novel treatment options for TNBC and other types of solid tumors currently unresponsive to conventional chemo- and immunotherapies.

One possible strategy to deal with TAM-mediated therapeutic resistance relies on depleting macrophages with anticolonystimulating factor receptor 1 (anti-CSF1R) antibodies.¹³ However, CSF1R is a pan-macrophage marker and



Received: March 2, 2020

Revised: May 14, 2020

Accepted: May 18, 2020

Published: May 18, 2020



expressed, besides the protumoral M2-skewed subset of TAMs, also by tumoricidal M1-like macrophages and normal tissue macrophages.^{14,15} Therefore, interventions aimed at modulating the CSF1/CSF1R axis are associated with severe side effects that originate from the systemic depletion of the CSF1-dependent macrophage pool not only in the tumor but also in normal tissues such as liver, skin, and colon.¹⁶ On the tumor response level, a limited therapeutic efficacy was observed for CSF1R-targeted therapies in patients,¹⁷ and anti-CSF1R treatment has even proven to be detrimental in some solid tumor models.¹⁸

The multiligand mannose receptor (CD206/MRC1) has emerged as an attractive and clinically relevant target on M2 TAMs.⁷ CD206 has three domains: a cysteine-rich domain (cysR) that binds to sulfated proteoglycans, a fibronectin type II domain (FNII) that interacts with collagen, and a lectin domain composed of 8 carbohydrate recognition domains (CTLDs) that bind mannose. One of the most widely used approaches for targeting CD206 is to use mannose-based molecules to engage CTLDs of the lectin domain.^{19,20} However, other mannose-binding proteins, such as CD209,^{21,22} are expressed in healthy tissues (such as intestinal tissue and genital mucosa²³), raising concerns on the specificity of mannose-based affinity ligands.

We recently identified a short homing peptide mUNO (sequence: CSPGAK) that targets the marker of M2-skewed macrophages, CD206.^{24–26} The parental peptide of mUNO, a cyclic disulfide-bridged peptide CSPGAKVRC (UNO), was identified by *in vivo* phage display on peritoneal macrophages of breast tumor-bearing mice.²⁴ UNO targeting of cytotoxic exosomes to M2 TAMs provided a therapeutic advantage in mice bearing TNBC, and the M2 TAM targeting was shown to be mediated by the interaction between UNO and CD206.²⁷

UNO is a CD206-targeting redox-responsive peptide, and its CD206 interaction required linearization of the peptide by the reducing tumor microenvironment, a reducing capacity which is not present in smaller tumors.²⁸ In subsequent studies, we focused on the linear version of UNO, mUNO, as its CD206 binding does not require a reducing environment. The peptide mUNO targeted M2 TAMs in advanced breast cancer,²⁴ cultured human M2 macrophages,²⁵ and recombinant human CD206 (hCD206).²⁵ Importantly, mUNO and mannose did not compete for the binding site on hCD206, suggesting the involvement of a different binding site. Indeed, computational studies revealed that the mUNO-binding epitope is located in a binding pocket between CTLD1 and CTLD2 domains of hCD206²⁵ that has no other reported ligands.

Here, we studied the ability of mUNO to target M2 TAMs in early-stage primary TNBC, in lung metastatic lesions of TNBC modeled in mouse and in spontaneous lung metastasis of TNBC. In addition, the interaction of mUNO with mouse CD206 (mCD206) was explored by *in silico* modeling, and cellular uptake and the fate of mUNO-targeted payloads were studied in human M2 macrophages *in vitro*.

■ EXPERIMENTAL SECTION

Umbrella Sampling Calculation. Simulations were performed using the Amber 18 simulation package,²⁹ with the ff14SB force field³⁰ and the TIP3P water model.³¹ The peptides used, mUNO and control (without FAM), were modeled using the tLeap module of AmberTools18, starting from their sequences. Coordinates used for human CD206 receptors were taken from the Protein Data Bank (PDB code:

SXTS).³² These coordinates, corresponding to the crystallographically determined human mannose receptor CD206, were used instead of the mCD206, since the latter was not yet resolved at the time of this study. Therefore, we modeled the mouse structure using the I-TASSER server^{33,34} and found a sequence identity value of 0.88 respect to human CD206 (SXTS) with full coverage of the modeled region (cysR, FNII, and two CTLD domains). The structural similarity found for the mouse and human receptors in the CTLD domains is illustrated in Figure S1 and justifies the use of the human structure for our calculations. Initial conformation for mUNO was taken from a previous molecular dynamics simulation. The systems consisted of the CD206 receptor, mUNO or control peptide, TIP3P water molecules, 0.1 M NaCl, and a Ca²⁺ atom, all immersed in a box 105 × 106 × 142 Å³. After minimizing, the box was equilibrated at 298 K and 1 atm for 1 ns. Finally, to compute the free energy of dissociation, umbrella sampling was performed using the distance between the receptor center of mass and the peptide center of mass as the reaction coordinate. Ten ns sampling was performed in a total of 74 windows separated 0.5 Å along the reaction coordinate. The potential of mean force (PMF) was constructed using WHAM with a bin size of 0.1 Å and a value for the iteration tolerance of 0.00001. Four simulations were performed, and the difference between them was used to calculate error bars.

Peptides. The peptides FAM-CSPGAK (referred to as FAM-mUNO), FAM-CAQK (referred to as FAM-control), and FAM-CGNKRTRGC (disulfide cyclized, referred to as FAM-LyP-1) were purchased from TAG Copenhagen (Frederiksberg, Denmark), where FAM is 5(6)-carboxyfluorescein, and it is coupled through an aminohexanoic acid spacer to the N-terminus of the peptides. The C-terminus of FAM-mUNO is free. Peptide solutions were prepared fresh each time to minimize peptide dimerization.

Cell Lines and Experimental Animals. 4T1 cells were purchased from ATCC (VA, USA). Cells were cultured in RPMI-1640 medium (Gibco by Life Technologies, cat. 72400-021) supplemented with 10% v/v fetal bovine serum (FBS, Capricorn Scientific, cat. FBS-11A) and 100 IU/mL penicillin–streptomycin (Capricorn Scientific, cat. PS-B) at +37 °C in the presence of 5% CO₂. In all animal experiments, 8–12-week-old female Balb/c mice were used. Animal experiment protocols were approved by the Estonian Ministry of Agriculture (project no. 48). All methods were performed in accordance with existing guidelines and regulations.

Tumor Models. Three TNBC tumor models were used: orthotopic model, where 1 × 10⁶ 4T1 cells in 50 μL of phosphate-buffered saline (PBS, Lonza, cat. 17–512F) were injected into mammary fat pad; lung foci model, where 5 × 10⁵ 4T1 cells were injected into the tail vein; and a spontaneous metastases model where 5 × 10⁴ 4T1 cells were injected orthotopically into the fourth mammary fat pad. In the orthotopic model, experiments were started when tumors reached 50 mm³; in the lung foci model, 10 days after inoculation when the mice started to show signs of sickness, such as difficulty in walking, dull or sluggish movements, and hunched posture; and in the spontaneous metastasis model, 26 days after inoculation. For biodistribution studies (orthotopic and lung foci), N = 3 mice were used for FAM-mUNO and FAM-control (total: 12); for *ex vivo* imaging studies, N = 3 mice were used for FAM-mUNO, FAM-LyP-1, and uninjected control (total: 9).

Synthesis and Functionalization of Polymersomes (PS).

The PS consisted of copolymer polyethylene glycol [molecular weight (Mw) 5000]-polycaprolactone (Mw 10 000) (PEG-PCL) and maleimide-polyethylene glycol (Mw 5000)-polycaprolactone (Mw 10 000) (Mal-PEG-PCL). Polymers were purchased from Advanced Polymer Materials Inc. (Canada). To form the FAM-mUNO-targeted PS (FAM-mUNO-PS), 8 mg of PEG-PCL and 2 mg of Mal-PEG-PCL were dissolved in 0.5 mL of acetone, and the organic solvent was evaporated with a nitrogen flow to form the polymer film. The film was hydrated with 1 mL of PBS (pH 7.4), and the PS was formed as previously described.³⁵ After PS formation, 2 equiv of FAM-mUNO (with respect to the Mal-PEG-PCL polymer) was dissolved in 0.1 mL of PBS, and the solution was added to the PS suspension. The sample was stirred for 2 h at room temperature (RT) and kept overnight at 4 °C. For the FAM-PS (control PS), the used protocol was the same as described, except mixing 8 mg of PEG-PCL and 2 mg of FAM-PEG-PCL to form the polymer film. FAM-PEG-PCL was synthesized as previously described.²⁴ The final PS samples had a concentration of 10 mg of polymer/mL. The PS samples were purified using size exclusion chromatography using a sepharose column (Sephacrose 4b, Sigma-Aldrich, 4B200) and PBS (pH 7.4) as an eluent. For the PS characterization, dynamic light scattering (DLS) (Zetasizer Nano ZS, Malvern Instruments, USA) and transmission electron microscopy (TEM) (Tecnai 10, Philips, The Netherlands) were used. For DLS, the PS samples were diluted with PBS (pH 7.4) until 1 mg/mL. Samples were scanned for 10 s at 173° and averaged over 10 runs. Measurements were repeated 3 times and averaged. For TEM, the PS samples were diluted in MQ water up to 0.1 mg/mL. The samples were placed on Formvar/carbon-coated copper grids 300 Mesh (Agar Scientific, U.K.) and stained using phosphotungstic acid water solution (0.75%, pH 7). For the binding studies, the concentration of PS was normalized for FAM.

The peptide density of FAM-mUNO in the PS composition was estimated. Serial dilutions of FAM-mUNO in PBS at different concentrations (20; 10; 5.1; 2.5; 1.3; 0.63 and 0.32 μM of the peptide) were prepared, and the fluorescence at 485 nm/535 nm was measured using a Victor X5Multilabel Microplate Reader (PerkinElmer, USA) to obtain a calibration curve. The fluorescence of the FAM-mUNO-PS sample in that same channel was measured (318241 au), and the concentration of FAM-mUNO in that sample was calculated using the calibration curve. The percentage of FAM-mUNO-PEG-PCL with respect to the total amount of polymer was 2.7 mol %. The fluorescence of FAM-mUNO-PS and control FAM-PS was the same (318241 au and 317230 au, respectively).

In Vitro Differentiation of Human M2 Macrophages.

Human primary blood mononuclear cells (PBMC) were purified from human blood buffy coat using Ficoll Paque Plus (GE Healthcare, cat. no. 17-1440-02) reagent and CD14⁺ microbeads (MACS Miltenyi Biotec, cat. 130-050-201). The buffy coat was mixed with PBS at +37 °C at a dilution 1:1–1.5. The diluted buffy coat (35 mL) was layered at a 45° angle over 10 mL of +37 °C Ficoll, and samples were centrifuged at 400g at RT for 35 min without any breaks to obtain correct layers. The PBMC layer was collected and washed with 30 mL of ice-cold washing buffer [2 mM ethylenediaminetetraacetic acid disodium salt (EDTA-Na, Sigma-Aldrich, cat. ED2SS-500G) dissolved in PBS] by centrifugation at 300g at RT for 10 min, followed by an additional wash with 40 mL of ice-cold washing

buffer and centrifugation at 200g at RT for 15 min to remove remaining platelets. The pellet was resuspended in 20 mL of ice-cold washing buffer and centrifuged at 300g at RT for 10 min. Equal volumes of 0.4% v/v Trypan blue (Smart Mix, cat. no. 3194) and cell suspension were combined and analyzed using TC10TM Automated Cell Counter (Bio-Rad). The supernatant was aspirated, and the pellet was dissolved in an ice-cold washing buffer (80 μL of buffer per 10⁷ cells). To isolate monocytes, CD14⁺ microbeads were added (20 μL of beads per 10⁷ cells). Cells and beads were mixed and incubated at +4 °C for 15 min, with gentle mixing every 5 min. The LS column (MACS Miltenyi Biotec, Cat. 130-042-401) was placed in a magnetic holder and rinsed with 3 mL of ice-cold washing buffer. After 15 min, the mixture of cells and beads was divided into two and loaded to the column. Columns were washed with 3 mL of ice-cold washing buffer 3 times. After the washes, columns were removed from the magnetic field, 5 mL of ice-cold washing buffer was added onto the column, and cells were flushed out using the plunger. A sample for cell counting was collected, and cells were centrifuged at 300g at RT for 10 min. Then 3.5 × 10⁵ cells in 500 μL of RPMI-1640 medium were seeded on a 24-well plate. Each well included FBS-coated glass coverslips. To obtain optimal macrophage attachment and polarization toward the M2 phenotype, IL-4 (50 ng/mL, BioLegend, cat. 574002) and M-CSF (100 ng/mL, BioLegend, cat. 574802) were added to the medium. The medium was replenished by substituting half of the medium with fresh medium containing IL-4 and M-CSF every other day for 6 days. To obtain M1 macrophages, the monocytes were incubated with M-CSF (100 ng/mL) for 6 days and then with LPS (100 ng/mL, Sigma-Aldrich, cat. L4391-1MG) and IFN-γ (20 ng/mL, BioLegend, cat. 570202) for 18 h. To obtain M0 macrophages, monocytes were incubated with M-CSF (100 ng/mL) for 6 days. The CD206 expression was confirmed by immunostaining for CD206 (dilution 1:200, hCD206, purified mouse antihuman CD206, BioLegend, cat. 321102), counterstaining with 4',6-diamidino-2-phenylindole (DAPI, Sigma-Aldrich, cat. D9542-5MG) (1 μg/mL in PBS), and analyzing the percentage of CD206⁺ cell population in M0, M1, and M2 samples using ImageJ software from images from 3 independent samples.

Uptake of Polymersomes in Human M2 Macrophages. Human M2 macrophages were obtained as described above, and 3.5 × 10⁵ cells were seeded on each well of a 24-well plate containing FBS-coated glass coverslips. Six days after seeding and stimulating the cells, one group received blocking with 10 μg/mL of the anti-hCD206 antibody for 2 h (without subsequent wash), and the other group did not. The M2 macrophages were incubated with FAM-mUNO-functionalized PS (FAM-mUNO-PS) or FAM-PS at a concentration of 1 mg/mL for 5 min. After incubation with PS, the cells were washed twice with RPMI-1640 medium and once with PBS, fixed with cold 4% w/v paraformaldehyde (PFA, Sigma-Aldrich, cat. P6148) for 10 min, and stained according to the immunofluorescence protocol. Cells were stained with rabbit anti-FITC (dilution 1:250, Invitrogen by Thermo Fisher Scientific, cat. A889) and mouse anti-hCD206 (dilution 1:200) and counterstained DAPI (1 μg/mL in PBS). For secondary antibodies, Alexa Fluor 647 goat antirabbit (goat antirabbit conjugated to the fluorophore Alexa Fluor 647) (dilution 1:400, Invitrogen by Thermo Fisher Scientific, cat. no. A21245) and Alexa Fluor 546 goat antimouse (goat antimouse conjugated to the

fluorophore Alexa Fluor 546) (dilution 1:300, Life Technologies, cat. no. A11003) were used. The coverslips were mounted using a mounting medium (Fluoromount-G Electron Microscopy Sciences, cat. no. 17984-25) and imaged using a Zeiss confocal microscope (Zeiss LSM-710) and 20× objective. The average fluorescence/CD206⁺ cell ratio was obtained using ImageJ from 6 pictures.

Pulse/Chase of FAM-mUNO Uptake. Human M2 macrophages were obtained as described above, and 3.5×10^5 cells were seeded on each well of a 24-well plate containing FBS-coated glass coverslips. On day 6 (after seeding and stimulation), the RPMI-1640 medium was removed and substituted with 300 μ L of fresh medium containing 3 nM of FAM-mUNO. Cells were placed in an incubator for 20 min, washed once with fresh medium, and chased for 5, 15, 30, 90, and 180 min. Subsequently, the cells were washed twice with media and once with PBS followed by fixation with cold 4% w/v PFA for 10 min. Fixed cells were immunostained with antibodies (1:200 dilution in 1% blocking buffer), 1% w/v bovine serum albumin (BSA, Capricorn Scientific, cat. BSA-1T), 1% v/v FBS and 1% v/v goat serum (Life Technologies, cat. 16210072) against Lamp1 (purified mouse antihuman CD107a, Biolegend, cat. 328601), Rab5 [mouse antihuman Rab5A (C-3), Santa Cruz Biotechnology, cat. Sc-515401], and Rab7 (purified rat antihuman Rab7A, BioLegend, cat. 850401), followed by staining with secondary antibodies and nuclear counterstaining with DAPI. Secondary antibodies used were Alexa Fluor 647 goat antirabbit (dilution 1:400, Invitrogen by Thermo Fisher Scientific, cat. A21245, for FAM), Alexa Fluor 546 goat antimouse (dilution 1:300, Invitrogen by Thermo Fisher Scientific, cat. A11003, for Lamp1 and Rab5), and Alexa Fluor 546 goat antirat (dilution 1:300, Life Technologies, cat. A11081, for Rab7). Glass coverslips were mounted using an aqueous mounting medium (Fluoromount-G Electron Microscopy Sciences) and imaged using a Zeiss confocal microscope and 63× objective, using the lowest optical thickness possible (pinhole: 60).

Stability of FAM-mUNO. The stability of FAM-mUNO (50 μ M) in RPMI-1640 supplemented with 10% v/v FBS was evaluated by reverse-phase high-performance liquid chromatography (RP-HPLC). At scheduled time points (0, 0.5, 1, 2, 3, 5, 8, and 24 h), 100 μ L aliquots were taken and diluted 1:1 using Milli-Q water, and 10 μ L of the final solution was injected in a Waters HPLC system provided with 2 \times 515 binary pumps, autosampler 717 Plus, FLD 2475, and PDA 2996. The reverse-phase (RP) C-18 Lichrospher analytical column (5 μ m, 25 \times 4.0 mm, Scharlab) was eluted with mQ water (eluent A) and acetonitrile (eluent B) both added to 0.05% v/v trifluoroacetic acid in a gradient mode from 10% to 90% eluent B in 18 min at a flow rate of 1 mL/min. The photodiode array detector was set at 450 nm, and FAM-mUNO eluted at 8 min. FAM-mUNO peaks were integrated using Empower 2.0 software (Waters). Time 0 h was considered as 100% of FAM-mUNO.

Determination of Blood Half-Life of Peptide. Healthy Balb/c mice were intravenously (i.v.) or intraperitoneally (i.p.) injected with FAM-mUNO. Ten μ L blood samples were obtained from the tail vein at different time points (0, 6, 10, 15, 30, 60, 180, 360 min and 24 h for i.v. administration and 0, 7, 10, 16, 30, 60, 120, 180, 360 min, and 24 h for i.p. administration) and mixed with 50 μ L of PBS-heparin solution. The blood samples were centrifuged at 300g for 5 min to separate plasma for fluorimetry of FAM using a plate reader

(FlexStation II Molecular Devices) at a 520 nm emission wavelength. $N = 3$ for both administration methods.

Peptide Biodistribution Studies. For homing studies, mice were injected i.p. with 30 nmoles of FAM-mUNO or FAM-control dissolved in 500 μ L of PBS. After 24 h, tissues were collected by anesthetizing the mice, followed by cervical dislocation. Tissues were fixed in cold 4% w/v PFA in PBS at +4 °C for 24 h, washed in PBS at RT for 1 h, and cryoprotected in 15% w/v sucrose (Sigma Life Science, cat. S9378-1KG) followed by 30% w/v sucrose at +4 °C overnight. Cryoprotected and fixed tissues were frozen in OCT (Optimal Cutting Temperature, Leica, cat. 14020108926), cryosectioned at 10 μ m on Superfrost+ slides (Thermo Fisher, cat. J1800AMNZ), and stored at -20 °C. For immunofluorescence, tissue sections were thawed and left to air-dry in the dark for at least 12 h to ensure optimal attachment to the glass. Air-dried tissue sections were rehydrated in PBS for 10 min, followed by permeabilization in PBS + 0.2% v/v Triton (Triton X-100, AppliChem, cat. A4975,0500) at RT for 10 min. Tissue slides were mounted into the immunostaining cassette, washed with PBST [PBS + 0.05% v/v Tween-20 (Sigma-Aldrich, cat. P1379)], and blocked with 5% blocking buffer (5% w/v BSA, 5% v/v FBS, and 5% v/v goat serum in PBST) at RT for 1 h. Primary antibodies diluted in 1% blocking buffer were added and incubated at +4 °C overnight. Incubation with secondary antibodies was at RT for 30 min, followed by washing and nuclear counterstaining with DAPI (1 μ g/mL in PBS) at RT for 5 min. FAM was detected using rabbit anti-FITC (dilution 1:100) and Alexa Fluor 647 goat antirabbit antibodies (dilution 1:200, Invitrogen by Thermo Fisher Scientific, cat. A21245). CD206 was detected using rat antimouse CD206 (dilution 1:100, Bio-Rad, cat. MCA2235GA) and Alexa Fluor 546 goat antirat antibodies (dilution 1:200, Life Technologies, cat. A11081). CD86 was detected using antimouse CD86 (dilution 1:100, BioLegend, cat. 105001) and Alexa Fluor-546 goat antirat antibodies (dilution 1:200, Life Technologies, cat. A11081). The coverslips were mounted using a mounting medium (Fluoromount-G Electron Microscopy Sciences, cat. 17984-25) and imaged using a Zeiss confocal microscope (Zeiss LSM-710) and 20× objective. Colocalization analysis was done using ImageJ and Pearson's coefficient, and average values were obtained from 3 tumors and at least 3 pictures from each tumor.

Ex Vivo Organ Imaging of Mice with Spontaneous Metastasis. Tumors were induced as described previously under the tumor models section. At day 26 postinoculation (p.i.), mice were injected i.p. with 30 nmoles of FAM-mUNO or FAM-LyP-1 dissolved in 500 μ L of PBS or left uninjected (uninjected control), and after 6 h, the mice were sacrificed, tumors and organs collected and fixed with cold 4% PFA overnight, and imaged using the IVIS Spectrum In Vivo Imaging System in the FAM channel fluorescence. After *ex vivo* imaging, tissues were cryoprotected and frozen in OCT, and 10 μ m sections were obtained and immunostained and imaged as described above in the section **Peptide Biodistribution Studies**.

Statistical Analysis. All statistical analyses were done using Origin Pro 8. Statistical significance was calculated using a one-way analysis of variance (ANOVA). Error bars represent the standard error.

RESULTS

In Silico Modeling Suggests That mUNO Interacts with the CTLD1/2 Domain of Mouse CD206. mUNO is known to target CD206 expressed on both human and mouse M2 macrophages. The binding site and mode of interaction of affinity ligands with their receptors are important, as it can allow the design of improved targeting ligands such as modified peptides with increased *in vivo* stability or low molecular weight peptidomimetic molecules.³⁶ Recently, we reported a computational study that revealed that the mUNO-binding epitope on hCD206 is located in a binding pocket between CTLD1 and CTLD2 domains.²⁵ However, the mode of interaction of mUNO with mCD206 has not been studied.

We calculated the free energy of unbinding of mUNO to mCD206 using the umbrella sampling method and compared it with the interaction of a control peptide of a similar Mw and the same charge (CAQK). In the case of mUNO, the lowest values of the potential of mean force (PMF), corresponding to the most stable pose were obtained for the peptide located in the CTLD1/2-binding pose reported for mUNO to hCD206²⁵ (Figure 1). The free energy needed for unbinding of mUNO to

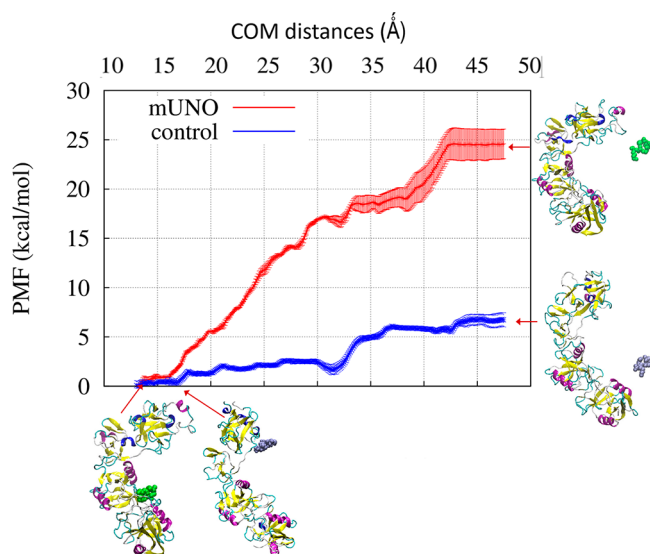


Figure 1. Potential of mean force from umbrella sampling calculations for mUNO and control. mUNO (green spheres) and the control peptide (lilac spheres) were placed at the binding pose located between lectin domains CTLD1 and CTLD2 and pulled apart using umbrella sampling calculations, increasing the center of mass separation of the peptide receptor until the unbound states were reached. Bound and unbound states for each peptide are illustrated. Error bars were calculated as the difference between four trajectories for each system.

mCD206 was ≈ 25 kcal/mol. In contrast, for the CAQK control peptide, the unbinding free energy was ≈ 7 kcal/mol, and its most stable pose was different from the starting pose (Figure 1), suggesting a low affinity of the control peptide for mCD206, and a significant difference with respect to mUNO.

FAM-mUNO Can Be Conjugated to Macromolecular Cargoes through Its Cysteine. For mUNO to be useful as a drug delivery vector, it must be amenable to conjugation without losing affinity for CD206. We have previously shown that mUNO can be conjugated to FAM (payloads other than FAM have not yet been investigated by us) through its N-terminus without affecting its targeting ability.^{24,25} To

investigate whether mUNO can be conjugated to a macromolecular cargo by its cysteine thiol without losing CD206-binding activity, we synthesized Nanosized polymeric vesicles (polymersomes, PS) bearing maleimide groups on the surface, and coupled to FAM-mUNO through a thiol-maleimide bond (schematized in Figure 2A); this gave a peptide density of FAM-mUNO on PS of 2.7 mol % (see methods). Both targeted and untargeted PS had a similar diameter (100–118 nm), as measured by DLS and TEM (Figure S2). FAM-mUNO-PS were incubated with primary human M2 macrophages, and confocal microscopy was used to study cellular uptake. We observed that the fluorescence/CD206⁺ cell was twice as high for FAM-mUNO-PS compared to untargeted FAM-PS (Figure 2B,C,G). A fraction of the binding and uptake of FAM-mUNO-PS was mediated by CD206, as preincubation of cells with anti-hCD206 reduced the uptake for FAM-mUNO-PS (Figure 2D,G) but not for FAM-PS (Figure 2E,G). The fraction of FAM-mUNO-PS uptake after blocking CD206 is suggested to be a receptor-independent uptake. Intriguingly, a-hCD206 not only did not reduce the uptake of FAM-PS but instead increased it (Figure 2G). Possibly the receptor-independent uptake fraction for both polymersomes was stimulated by the a-hCD206/hCD206 interaction, as was recently shown to occur for the interaction of CD206 with a peptide.³⁷ The signal of FAM-mUNO-PS inside the CD206⁺ cells was not diffuse and mainly appeared associated with CD206⁺ compartments/structures (Figure 2F). Intracellular CD206⁺ structures of a similar size and shape to the ones shown here were observed by others during the phagocytosis of parasites by CD206⁺ macrophages *in vitro*.³⁸ To show that *in vitro* FAM-mUNO provides selectivity to M2 macrophages, we evaluated the binding of FAM-mUNO-PS to M2 and M0 macrophages in parallel and observed significantly higher binding in M2 macrophages (Figure S3).

These studies showed that mUNO retained its CD206-binding activity when coupled to payloads using the thiol group of its cysteine.

Internalized FAM-mUNO in CD206⁺ M2 Macrophages Is Rescued from Lysosomal Entrapment.

The development of mUNO as an intracellular precision delivery vehicle requires a detailed understanding of its subcellular fate upon cell binding and internalization. To this aim, we performed pulse/chase experiments by incubating primary human M2 macrophages with FAM-mUNO for 20 min and monitored the fate of FAM in the context of markers of early endosomes, late endosomes, and lysosomes at different time points after the pulse. Under the conditions used here, 70% of the M2-differentiated macrophages became positive for CD206 expression (Figure S4). To make sure that our observations would be a consequence of the interaction of M2 macrophages with FAM-mUNO and not with a complex of the peptide with serum proteins, or degraded or dimerized FAM-mUNO, we first analyzed the stability of FAM-mUNO in this cell medium containing 10% FBS using RP-HPLC. We found negligible degradation or complex formation of FAM-mUNO at the incubation time point used herein (20 min) (Figure S5); hence, the following results can be ascribed to the interaction between FAM-mUNO and the cell membrane of M2 macrophages.

Confocal microscopy revealed, that at 5 min, a significant fraction of the peptide associated with early endosomes (white arrowheads in Figure 3A) and the peptide signal appeared mainly concentrated in round structures that were not late

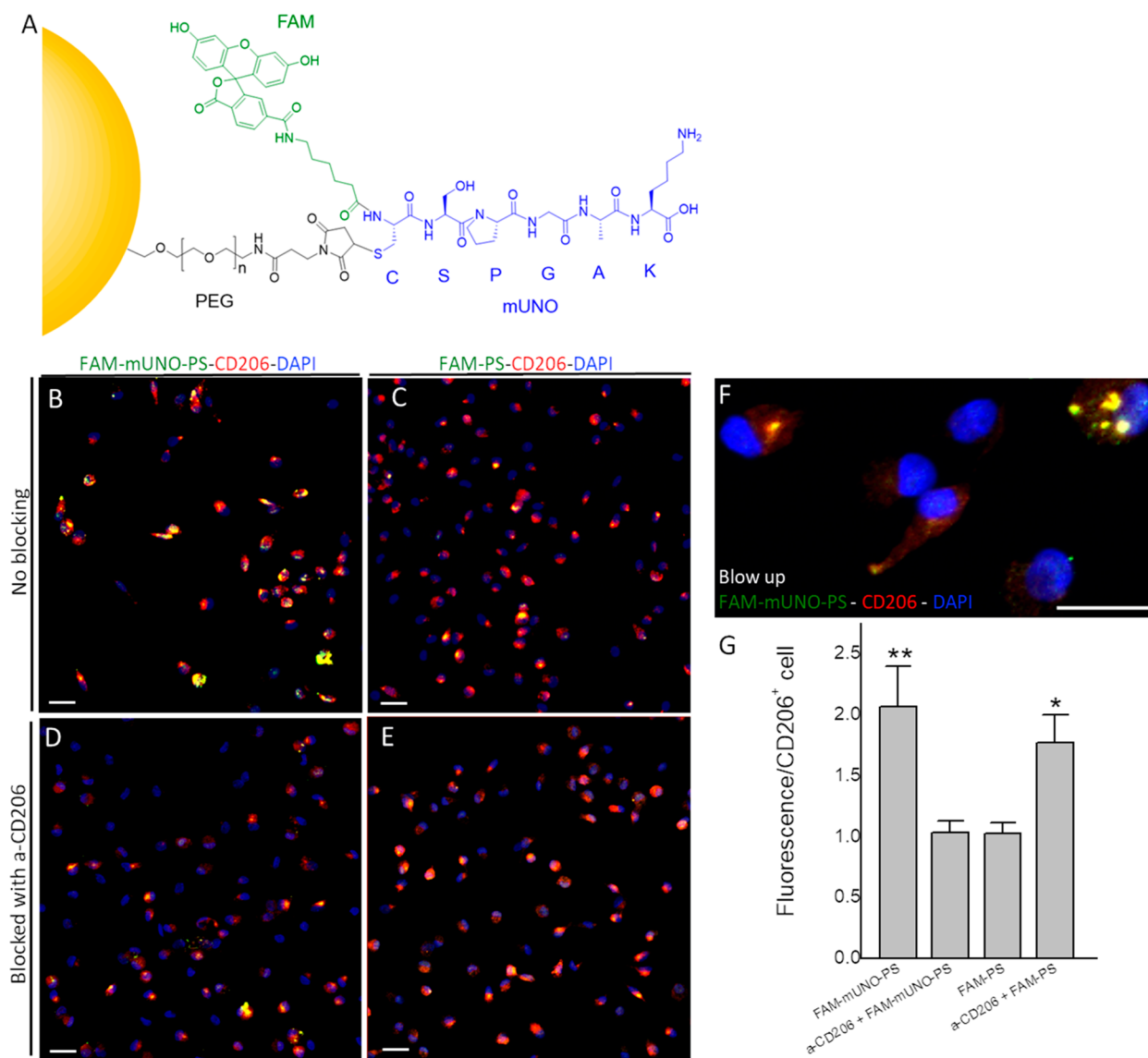


Figure 2. FAM-mUNO-PS targeting of primary human M2 macrophages. Schematic representation of the conjugation between FAM-mUNO (FAM-linker in green, mUNO in blue) and PEG-maleimide (in black) on the polymersomes (in yellow) (A). Human M2-skewed macrophages (see Materials and methods) were incubated with FAM-mUNO-PS or FAM-PS for 5 min, washed, fixed, permeabilized, stained with antibodies against FAM and CD206, and counterstained with DAPI. Binding of FAM-mUNO-PS and FAM-PS to CD206⁺ cells (B, C, respectively). Binding of FAM-mUNO-PS and FAM-PS, where the cells have been preincubated with the anti-hCD206 antibody (D, E, respectively). Blow up of FAM-mUNO-PS associated with CD206⁺ inside the cell (F). Quantification of the fluorescence/CD206⁺ cell using ImageJ (G). All scale bars: 20 μ m. ** $P \leq 0.01$, *** $P \leq 0.001$

endosomes (Figure 3F) or lysosomes (Figure 3K). Then, 15 min after the incubation, a smaller fraction of the peptide associated with Rab5⁺ early endosomes and the remaining FAM-mUNO signal appeared diffusely inside the cell (Figure 3B) and was not associated with late endosomes (Figure 3G) or lysosomes (Figure 3L). A lower degree of overlap of FAM-mUNO fluorescence with early endosomes was observed at later time points (Figure 3C–E). No colocalization of the FAM-mUNO signal was seen at any time point with markers of late endosomes (Rab7⁺) (Figure 3F–J) or lysosomes (Lamp1⁺) (Figure 3K–O).

These results support the idea that FAM-mUNO is internalized through endosomal uptake and showed that, in M2 macrophages, mUNO-targeted drugs do not undergo lysosomal sequestration.

Effect of Administration Route on Pharmacokinetics and Bioavailability of FAM-mUNO.

To address the effect of the administration route on the blood bioavailability of FAM-mUNO, we performed comparative studies using i.p. and i.v. administration routes on healthy Balb/c mice.

We observed that the administration route has a profound effect on the pharmacokinetics of FAM-mUNO (Figure 4A). The plasma concentration of i.v. injected FAM-mUNO showed a biphasic exponential decay, whereas the concentration of i.p. injected FAM-mUNO displayed an initial increase, reached a maximum at 30 min, and then decayed over time. These profiles agree with those reported for other compounds of similar Mw given i.p. and i.v.³⁹

Compared to the i.v. administration route, the half-life for the i.p. injected peptide was ~ 4 times higher (Figure 4B), and

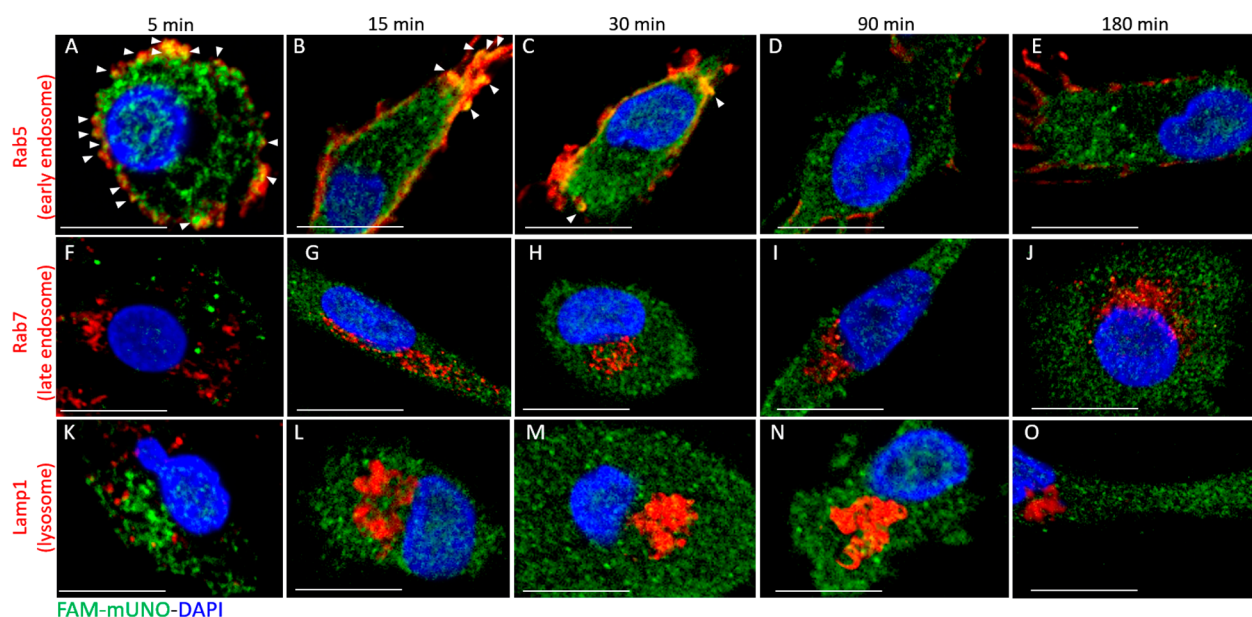


Figure 3. Subcellular fate of FAM-mUNO. Confocal microscopy images of M2 macrophages derived from human blood incubated with FAM-mUNO for 20 min, washed, chased for 5, 15, 30, 90, and 180 min, washed, fixed, and immunostained against FAM (shown in green) and Rab5 (A–E, shown in red), Rab7 (F–J, shown in red), or Lamp1 (K–O, shown in red). Images were taken using a Zeiss confocal microscope and 63× objective, using the lowest optical thickness possible (pinhole: 60). Cells stained with only the secondary antibodies imaged under the same imaging conditions are shown in Figure S6. Scale bars represent 10 μm , $N = 5$.

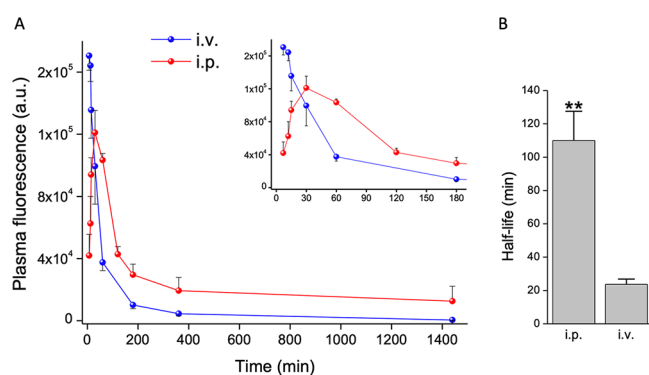


Figure 4. Bioavailability in blood for FAM-mUNO administered via the intraperitoneal route vs intravenous route. Thirty nmoles of FAM-mUNO dissolved in PBS were injected i.v. or i.p. in Balb/c mice ($N = 3$), and blood was withdrawn at different time points. Blood was mixed with PBS-heparin, centrifuged to obtain plasma, and FAM fluorescence measured using a plate reader at 520 nm as the emission wavelength. Panel A: FAM fluorescence of blood plasma collected at different time points after i.v. injection (blue curve) and i.p. injection (red curve). Panel B: half-life values obtained from the i.p. curve of panel A and from fitting i.v. data with a biexponential decay equation. $**P < 0.01$.

the area under the curve (a measure of the amount of available peptide in the blood) for i.p. was ~ 3.6 -fold higher.

The superior pharmacokinetics and higher bioavailability of the peptide when using i.p. administration supports the use of the i.p. administration route for mUNO-guided compounds.

Intraperitoneal FAM-mUNO Targets M2 TAMs in Early-Stage Orthotopic TNBC and in Lung Foci of TNBC. We were interested in evaluating whether FAM-mUNO could be used to target M2 TAMs in early-stage orthotopic TNBC and in lung foci of TNBC. Immunostaining confirmed the presence of M1 and M2 TAMs in the orthotopic tumor and lung foci (Figure S7A–F). In malignant tissue in both

models, M2 TAMs were greatly overrepresented [M2/M1 TAM ratio ~ 12 for the orthotopic model and ~ 7 for the lung foci (Figure S7G)]. Increasing the digital gain settings in the confocal microscopy images of healthy lungs revealed the presence of CD206⁺ cells (Figure S8A), as expected and consistent with the presence of CD206⁺ alveolar macrophages in the normal lungs.⁴⁰

Twenty-four h after i.p. administration, FAM-mUNO showed accumulation in M2 TAMs of early-stage orthotopic breast tumors (Figure 5A) and of lung foci (Figure 5G) and low association with M1 TAMs (Figure 5C,I). No accumulation of FAM-mUNO occurred in CD206[−] regions of lungs with foci (Figure 5L). To confirm that the selectivity observed was due to mUNO, we performed parallel experiments using FAM-control. FAM-control showed a low association with M2 TAMs and M1 TAMs, respectively, in both models (Figure 5B,D,H,J). FAM-control showed some positive staining, possibly associated with the presence of chondroitin sulfate proteoglycans, known receptors for the CAQK peptide,⁴¹ in this breast model.^{42,43}

Importantly, FAM-mUNO showed low liver accumulation (Figure S9A,C), in accordance with the low expression of CD206 in hepatic tissue. FAM-control also showed no liver accumulation (Figure S9B,D), which was expected, as its receptors are not expressed in the liver.⁴¹ In line with the pharmacokinetics results, FAM-mUNO showed better homing to M2 TAMs when administered intraperitoneally than when using intravenous administration (Figure 5F). Additionally, a simple calculation of the number of CD206 receptors in peritoneal cavity cells of 4T1 mice (6% of peritoneal cavity cells being CD206⁺,²⁴ and each expressing 2.5×10^4 copies of CD206⁴⁴) revealed that the peptide administered (30 nmoles) was in large excess with respect to the number of receptors; therefore, the CD206⁺ macrophages present in the peritoneal cavity may not alter the dose of FAM-mUNO that reaches the blood.

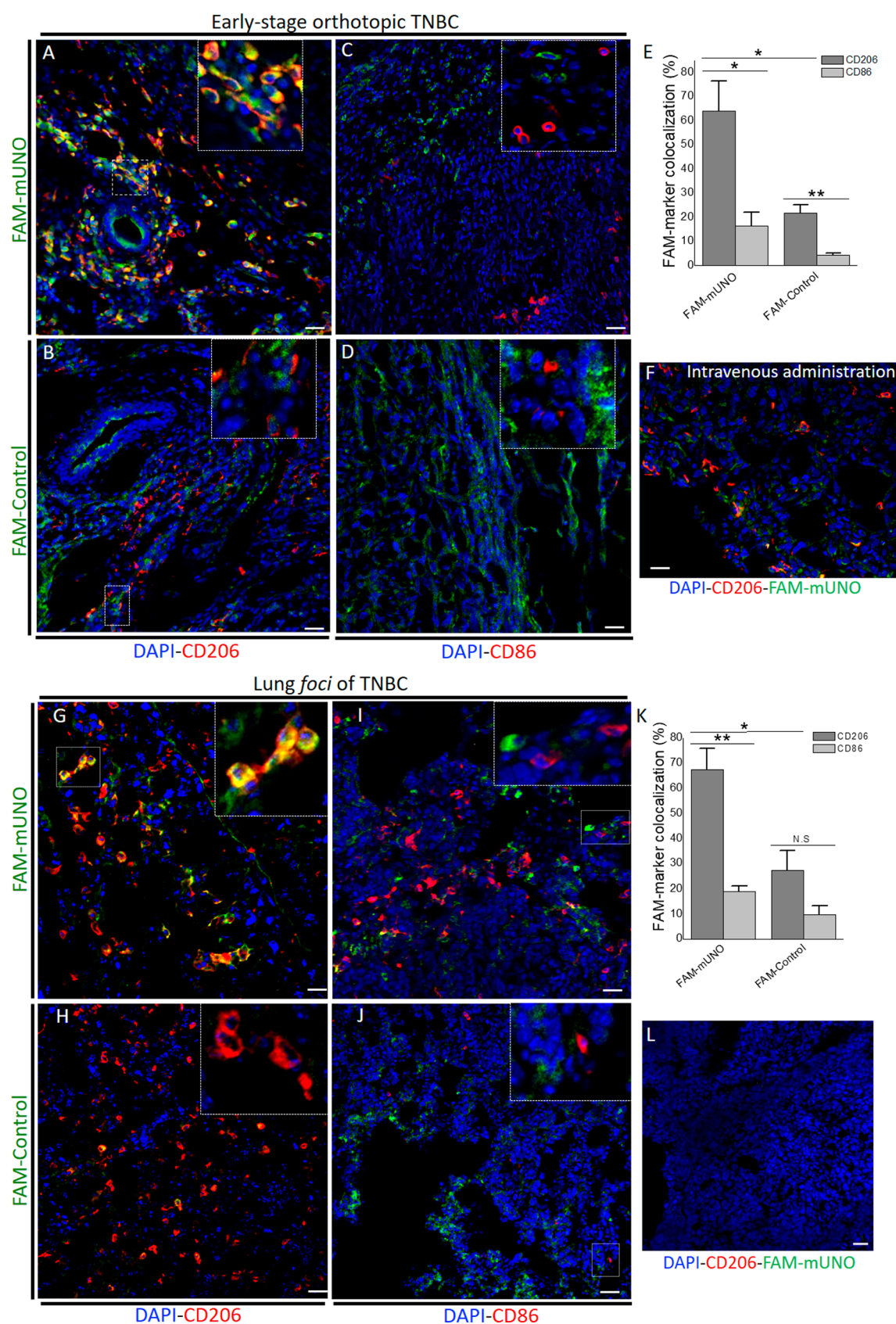


Figure 5. FAM-mUNO targets M2 TAMs in early-stage orthotopic TNBC and in lung foci of TNBC. 30 nmol of FAM-mUNO or FAM-control were injected i.p. (or i.v. in panel F) and left to circulate for 24 h. At 24 h, the mice were sacrificed, and the organs were collected, fixed, cryoprotected, sectioned, and immunostained for FAM (shown in green) and CD206 or CD86 (shown in red). FAM-mUNO colocalized with M2 TAMs in the orthotopic tumor and in the lung foci of TNBC (A and G, respectively) in contrast to FAM-control (B and H). CD86 staining showed that FAM-mUNO did not colocalize with CD86⁺ cells in either the orthotopic tumor or the lung foci (C and I). For both models, the

Figure 5. continued

FAM-CD206 colocalization index (Pearson's coefficient) was approximately 65% for mUNO and 15–20% for control (E and K, respectively). No accumulation of FAM-mUNO was observed in CD206[−] regions of these lungs (L). Scale bars represent 20 μm . * $P \leq 0.05$, ** $P \leq 0.01$, N.S. = not significant.

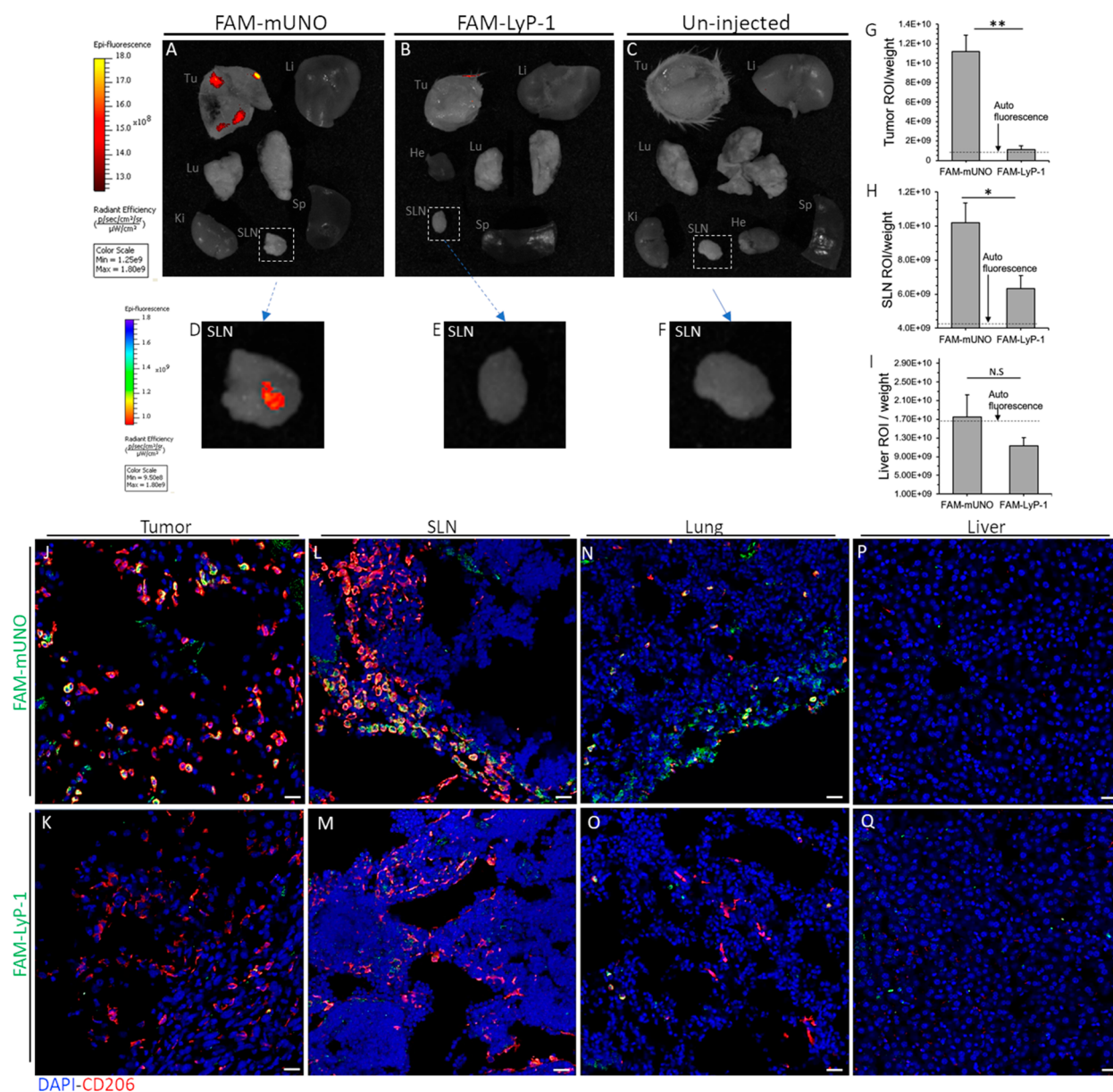


Figure 6. FAM-mUNO detects lymph nodes and M2 TAMs of mice with spontaneous lung metastasis. 30 nmoles of FAM-mUNO or FAM-LyP-1 were injected i.p. in 4T1 tumor-bearing mice with spontaneous lung metastasis and left to circulate for 6 h. At 6 h, the mice were sacrificed, the organs were collected, fixed overnight, and imaged with the IVIS Spectrum In Vivo Imaging System in the FAM channel fluorescence (A and B for FAM-mUNO and FAM-LyP-1, respectively, and C for the uninjected control). The fluorescence of the tumor, SLN, and liver was measured, normalized to their weights, and graphed (G–I). * $P \leq 0.05$, ** $P \leq 0.01$, N.S. = not significant. Immunofluorescence staining of FAM and CD206 of the tissues imaged in panels A and B (J–Q). Scale bars represent 20 μm .

FAM-mUNO Detects the Lymph Node and M2 TAMs of Mice with Spontaneous Lung Metastasis. To evaluate the potential applications of mUNO, we performed whole organ fluorescence imaging, in the FAM channel, of 4T1 tumor-bearing mice with spontaneous lung metastasis (Figure S10), i.p. administered with FAM-mUNO 6 h before. To compare the performance of mUNO to another validated TAM targeting agent, we used the peptide LyP-1, which homes

to TAMs,^{45,46} and also lymphatic vessels of tumors.^{47,48,46,49,50} FAM-mUNO was able to detect the tumor and the sentinel lymph node (SLN) (Figure 6A,D,G,H), whereas the signal in those tissues from FAM-LyP-1 (Figure 6B,E,G,H) did not differ from the tissue autofluorescence levels (Figure 6C,F,G,H). Additionally, the peptide signal in the liver for both FAM-mUNO and FAM-LyP-1 did not differ significantly and was within the liver autofluorescence values (Figure 6I).

The FAM signals from the tumor and SLN in the FAM-mUNO-injected mice associated with M2 macrophages in those tissues (Figure 6J,L, respectively). No evident FAM signal was detected with immunofluorescence in the tumor and SLN of mice injected with FAM-LyP-1 (Figure 6K,M, respectively). Even if the sensitivity of the FAM whole organ imaging studies was insufficient to pick up the signal from the lungs, immunofluorescence processing showed homing of FAM-mUNO to M2 TAMs of this spontaneous lung metastasis (Figure 6N) as opposed to FAM-LyP-1 (Figure 6O). In line with previous results described in this paper, no FAM signal was observed in the livers using immunofluorescence (Figure 6P,Q).

While FAM is not the most suited live imaging probe, due to high tissue absorption and scattering in this spectral region, these results prove the concept that mUNO can serve as a diagnostic probe for metastatic dissemination, by guiding an imaging agent that detects a signal from M2 TAMs and SLN, more sensitively than an established TAM/SLN targeting agent.

DISCUSSION

Targeting the pro-tumoral macrophages while leaving healthy organs untouched remains a challenge. Most of the ongoing 13 clinical studies focus on depleting CSF1R⁺ macrophages to potentiate chemotherapy or checkpoint immunotherapy.¹³ Because CSF1R is present in the healthy brain (in the microglia) and on non-M2 macrophages, alternatives to CSF1R-based targeting strategies are needed. It was recently shown that in melanoma, the depletion of CD163⁺ TAM population alone, using anti-CD163-coated liposomal doxorubicin, generated an effective therapeutic effect.⁵¹ Targeting CXCR4 on macrophages using the CXCR4 antagonist plerixafor has provided therapeutic effect in a Lewis lung carcinoma model.¹² In humans, the chemokine receptor CCR2 of macrophages has been targeted using the CCR2 inhibitor PF-04136309.⁵² Condeelis et al. have shown that targeting another receptor of M2 TAMs, TIE2, using the TIE2 inhibitor rebastinib, blocked their function and inhibited metastasis in a breast cancer model.⁵³

In metastatic breast cancer, CD206⁺ TAMs are angiogenic, relapse-stimulating,^{7,12} and metastasis-promoting.^{9–11} Whereas multiple studies have reported targeting CD206 using mannose and its analogues, mannose binds to other receptors such as CD209^{21,22} that is highly expressed in the intestinal tissue and in genital mucosa.²³

Here, we demonstrate that mUNO, a CD206-binding peptide, can be used for specific targeting of M2 TAMs in early-stage triple-negative primary breast tumors and in metastatic lesions, with minimal liver accumulation. In contrast, our control peptide of a similar sequence and molecular weight and the same charge as mUNO showed no targeting to M2 TAMs under the same conditions. The minimal liver accumulation of FAM-mUNO was in line with the low expression observed for its binding partner, CD206. The bioavailability of i.p. administered FAM-mUNO in the blood was 3.6-fold higher than when administered i.v. The longer plasma half-life and higher bioavailability following i.p. administration are the likely explanations for the superior M2 TAM targeting observed for this route. CD206-binding nanobodies have been reported to show M2-TAM uptake and also liver accumulation.⁵⁴ The higher permeability and retention that occurs in tumors, combined with the low affinity

of a peptide, with respect to a nanobody, might explain why FAM-mUNO only targeted CD206 in the tumor and not in the liver.

On hCD206, mUNO does not bind the mannose-binding site but an epitope located between CTLD1 and CTLD2.²⁵ Here, molecular modeling suggested that also in the case of mCD206, mUNO interacts with the interlectin domain. This suggests that, compared to mannose-based M2 TAM targeting strategies, mUNO may have fewer off-target effects. To validate the binding site predicted by our modeling studies, it will be of interest to perform binding studies to the wild-type CTLD1–2 fragment of CD206 and to variants where the amino acids predicted to participate in the binding have been mutated.

Our study shows that mUNO can be coupled to nanoparticle cargoes through the side chain of its cysteine without losing its ability to interact with CD206. Polymersomes coated with FAM-mUNO by a thiol-maleimide bond showed increased CD206-dependent uptake by M2 TAMs. The use of other bonds such as a disulfide bond is also expected to be feasible. Polymersomes are versatile nanocarriers that can be loaded with both hydrophilic and hydrophobic cargoes.⁵⁵ In the past, we have used radiolabeled peptide-guided PEG–PCL polymersomes for early detection of triple-negative breast tumors by PET imaging.³⁵ In the past, we have used another class of polymeric vesicles, pH-sensitive, endosomolytic poly(oligoethylene glycol methacrylate)-poly(2-(diisopropylamino)ethyl methacrylate) (POEGMA-PDPA) polymersomes, for affinity targeting studies to treat metastatic gastric cancer in mice.^{56–58} In the follow-up studies, it will be of interest to study if mUNO functionalized POEGMA-PDPA polymersomes show a more efficient cytosolic release than possible with PEG–PCL polymersomes for improved M2 TAM-targeted theranostics.

The rationale for the peptide density on PS selected here is based on our previous studies using radiolabeled peptide-targeted PEG–PCL polymersomes to target 4T1 tumors in mice.³⁵ Those biodistribution studies showed a remarkable accumulation of the peptide-targeted PS in the tumor of 26% ID/g. Motivated by that high tumor accumulation, we decided to replicate herein that synthesis and peptide density (2–3 mol %). We have previously shown that the peptide density is an important parameter that affects the binding of peptide-targeted nanoparticles to cells expressing the peptide receptor.⁵⁹ In that study, we showed that an intermediate peptide density of 2.5–5 mol % yielded the optimal binding and uptake and that a higher peptide density resulted in decreased binding. The peptide density is therefore expected to also alter the biodistribution and tumor accumulation of FAM-mUNO-PS.

High-magnification confocal microscopy studies showed that, in M2 macrophages, internalized FAM-mUNO avoids getting trapped in lysosomes. Macrophage internalization by engaging the lectin domain of CD206 has been shown to avoid lysosomal routing,⁶⁰ whereas ligands that engage the fibronectin domain of CD206 are routed to lysosomes.⁶¹ Our studies encourage uses for mUNO to guide to M2 TAMs cytosolically acting apoptogenic drugs such as doxorubicin or daunorubicin,⁶² or agents for the transformation to M1 TAMs such as microRNA 155,⁶³ or small interfering RNA (siRNA) to knockdown the endoribonuclease DICER.⁶⁴ Early endosomal localization of mUNO is consistent with receptor-mediated endocytosis and opens additional therapeutic possibilities, such

as the delivery of agonists of Toll-like receptor 7/8 (TLR7/8) on the endosomal membrane. The delivery of TLR7/8 agonists, such as resiquimod to macrophages, has recently proven to be a promising way to treat melanoma.^{65,22} However, in those studies, the TLR7/8 ligand was not targeted to the M2 subset, and high doses of resiquimod were necessary to achieve a response.

The fact that FAM-mUNO targeted M2 TAMs in metastatic lesions and primary breast tumors with low liver accumulation suggests the possibility to use mUNO as a radioligand, i.e., to carry therapeutic radioisotopes like ¹⁷⁷Lu, by conjugating the chelating agent dodecanetetraacetic acid (DOTA) to its N-terminus, with the aim of depleting M2 TAMs and the surrounding tissue. In fact, a low Mw ligand targeting the prostate-specific membrane antigen PSMA, coupled to ¹⁷⁷Lu-DOTA, is in phase III clinical trials for castration-resistant prostate cancer (clinical trial identifier: NCT03511664).

Our whole organ imaging studies showed the potential of mUNO as a diagnostic tool, to monitor M2 TAMs and metastatic progress through sentinel lymph node imaging, if FAM is replaced with a near-infrared fluorophore (such as IRDye800CW⁶⁶) or DOTA chelating a PET active radioisotope like ⁶⁸Ga.

Additionally, mUNO would allow contrasted PET imaging to detect metastatic foci. Indeed, peptide-based imaging probes currently being developed show translational promise,^{26,67} like the nonamer peptide that targets EDB-FN (fibronectin extra domain B), or an integrin-targeting peptide, both conjugated to a ⁶⁸Ga-chelating PET-active probe for imaging of prostate cancer,⁶⁸ and head and neck squamous carcinoma and non-small cell lung cancer in humans,⁶⁹ respectively.

CONCLUSIONS

We showed here that (1) mUNO appears to target a newly identified binding site in the CTLD1/2 region of mCD206, distinguishing it from mannose-based ligands; (2) cargo can be coupled to mUNO using the lateral chain of the cysteine without losing CD206-binding; (3) low Mw cargo conjugated to the N-terminus of mUNO avoids lysosomal entrapment; (4) the administration route is determining for targeting, having the intraperitoneal route superior pharmacokinetics and superior M2 TAM targeting; (5) mUNO can be used to precisely target M2 TAMs of triple-negative breast tumors at an early stage and also of their lung foci; (6) in *ex vivo* imaging, FAM-mUNO could detect the sentinel lymph node and M2 TAMs in mice with metastasized TNBC more sensitively than a validated TAM targeting agent. Collectively, these studies warrant theranostic applications of mUNO in triple-negative breast cancer.

ASSOCIATED CONTENT

Supporting Information

The Supporting Information is available free of charge at <https://pubs.acs.org/doi/10.1021/acs.molpharmaceut.0c00226>.

Structural prediction of mouse CD206 compared with the human crystallographic structure (PDB code: 5XTS); characterization of FAM-mUNO-PS and FAM-PS; binding of FAM-mUNO-PS to primary human M2 and M0 macrophages; CD206 characterization of primary human macrophages; stability of FAM-mUNO in RPMI supplemented of 10% FBS; secondary antibody

control for pulse/chase study; M1 and M2 TAMs in 4T1 tumor models; CD206⁺ cells in lungs of healthy Balb/c mice; FAM-mUNO and FAM-control show low presence in liver; spontaneous lung metastasis in the 4T1 model (PDF)

AUTHOR INFORMATION

Corresponding Authors

Tambet Teesalu – Laboratory of Cancer Biology, Institute of Biomedicine and Translational Medicine, University of Tartu, Tartu 50411, Estonia; Center for Nanomedicine and Department of Cell, Molecular and Developmental Biology, University of California, Santa Barbara, California 93106, United States; Cancer Research Center, Sanford Burnham Prebys Medical Discovery Institute, La Jolla, California 92037, United States; Phone: +372-53974441; Email: tambet.teesalu@ut.ee

Pablo Scodeller – Laboratory of Cancer Biology, Institute of Biomedicine and Translational Medicine, University of Tartu, Tartu 50411, Estonia; orcid.org/0000-0003-0745-2467; Phone: +372-7374268; Email: pablo.david.scodeller@ut.ee

Authors

Anni Lepland – Laboratory of Cancer Biology, Institute of Biomedicine and Translational Medicine, University of Tartu, Tartu 50411, Estonia

Eliana K. Ascuitto – School of Science and Technology, National University of San Martín (UNSAM) and CONICET, Campus Migueletes, San Martín, Buenos Aires CP 1650, Argentina

Alessio Malfanti – Polymer Therapeutics Laboratory, Centro de Investigación Príncipe Felipe, Valencia 46012, Spain

Lorena Simón-Gracia – Laboratory of Cancer Biology, Institute of Biomedicine and Translational Medicine, University of Tartu, Tartu 50411, Estonia

Valeria Sidorenko – Laboratory of Cancer Biology, Institute of Biomedicine and Translational Medicine, University of Tartu, Tartu 50411, Estonia

Maria J. Vicent – Polymer Therapeutics Laboratory, Centro de Investigación Príncipe Felipe, Valencia 46012, Spain; orcid.org/0000-0001-7771-3373

Complete contact information is available at:

<https://pubs.acs.org/10.1021/acs.molpharmaceut.0c00226>

Funding

P.S. was supported by the Estonian Research Council (grant: PUT PSG38 to P.S.) and a proof-of-concept grant from the development fund of Tartu University. E.A. acknowledges resources provided by the CYTED cofunded Thematic Network RICAP (517RT0529). A.L. and V.S. acknowledge a Ph.D. fellowship from the Estonian government. L.S.G. acknowledges a mobilitas grant from the Estonian Research Council (MOBJD11). T.T. was supported by the European Regional Development Fund (project no. 2014-2020.4.01.15-0012), and Estonian Research Council (grants PRG230 and EAG79).

Notes

The authors declare no competing financial interest.

ACKNOWLEDGMENTS

We thank Gemma Carreras-Badosa and Ana Rebane for their help with setting up the *in vitro* macrophage model used here.

■ REFERENCES

- (1) Foulkes, W. D.; Smith, I. E.; Reis-Filho, J. S. Triple-negative breast cancer. *N. Engl. J. Med.* **2010**, *363*, 1938.
- (2) Carey, L.; Winer, E.; Viale, G.; Cameron, D.; Gianni, L. Triple-negative breast cancer: Disease entity or title of convenience? *Nat. Rev. Clin. Oncol.* **2010**, *7*, 683.
- (3) Henschel, V.; Loi, S.; Im, S.-A.; Chui, S. Y.; Emens, L. A.; Hegg, R.; Iwata, H.; Rugo, H. S.; Husain, A.; Schmid, P.; Molinero, L.; Diéras, V.; Shaw Wright, G.; Winer, E. P.; Schneeweiss, A.; Funke, R.; Barrios, C. H.; Adams, S. Atezolizumab and Nab-Paclitaxel in Advanced Triple-Negative Breast Cancer. *N. Engl. J. Med.* **2018**, *379*, 2108.
- (4) Scodeller, P. Hyaluronidase and other Extracellular Matrix Degrading Enzymes for Cancer Therapy: New Uses and Nano-Formulations. *J. Carcinog. Mutagen.* **2014**, *05*, 1–5.
- (5) Neubert, N. J.; Schmittnaegel, M.; Bordry, N.; Nassiri, S.; Wald, N.; Martignier, C.; Tillé, L.; Homicsko, K.; Damsky, W.; Maby-El Hajjami, H.; Klamann, I.; Danenberg, E.; Ioannidou, K.; Kandalaf, L.; Coukos, G.; Hoves, S.; Ries, C. H.; Fuertes Marraco, S. A.; Foukas, P. G.; De Palma, M.; Speiser, D. E. T cell-induced CSF1 promotes melanoma resistance to PD1 blockade. *Sci. Transl. Med.* **2018**, *10*, eaan3311.
- (6) Peranzoni, E.; Lemoine, J.; Vimeux, L.; Feuillet, V.; Barrin, S.; Kantari-Mimoun, C.; Bercovici, N.; Guérin, M.; Biton, J.; Ouakrim, H.; Régnier, F.; Lupo, A.; Alifano, M.; Damotte, D.; Donnadieu, E. Macrophages impede CD8 T cells from reaching tumor cells and limit the efficacy of anti-PD-1 treatment. *Proc. Natl. Acad. Sci. U. S. A.* **2018**, *115*, E4041.
- (7) Gordon, S. R.; Maute, R. L.; Dulken, B. W.; Hutter, G.; George, B. M.; McCracken, M. N.; Gupta, R.; Tsai, J. M.; Sinha, R.; Corey, D.; Ring, A. M.; Connolly, A. J.; Weissman, I. L. PD-1 expression by tumour-associated macrophages inhibits phagocytosis and tumour immunity. *Nature* **2017**, *545*, 495–499.
- (8) Hartley, G. P.; Chow, L.; Ammons, D. T.; Wheat, W. H.; Dow, S. W. Programmed Cell Death Ligand 1 (PD-L1) Signaling Regulates Macrophage Proliferation and Activation. *Cancer Immunol. Res.* **2018**, *6*, 1260.
- (9) Harney, A. S.; Arwert, E. N.; Entenberg, D.; Wang, Y.; Guo, P.; Qian, B. Z.; Oktay, M. H.; Pollard, J. W.; Jones, J. G.; Condeelis, J. S. Real-time imaging reveals local, transient vascular permeability, and tumor cell intravasation stimulated by TIE2hi macrophage-derived VEGFA. *Cancer Discovery* **2015**, *5*, 932–943.
- (10) Kitamura, T.; Doughty-Shenton, D.; Cassetta, L.; Fraggogianni, S.; Brownlie, D.; Kato, Y.; Carragher, N.; Pollard, J. W. Monocytes differentiate to immune suppressive precursors of metastasis-associated macrophages in mouse models of metastatic breast cancer. *Front. Immunol.* **2018**, *8*, 1.
- (11) Wyckoff, J. B.; Wang, Y.; Lin, E. Y.; Li, J. F.; Goswami, S.; Stanley, E. R.; Segall, J. E.; Pollard, J. W.; Condeelis, J. Direct visualization of macrophage-assisted tumor cell intravasation in mammary tumors. *Cancer Res.* **2007**, *67*, 2649–2656.
- (12) Hughes, R.; Qian, B. Z.; Rowan, C.; Muthana, M.; Keklikoglou, I.; Olson, O. C.; Tazzyman, S.; Danson, S.; Addison, C.; Clemons, M.; Gonzalez-Angulo, A. M.; Joyce, J. A.; De Palma, M.; Pollard, J. W.; Lewis, C. E. Perivascular M2 macrophages stimulate tumor relapse after chemotherapy. *Cancer Res.* **2015**, *75*, 3479–3491.
- (13) Pathria, P.; Louis, T. L.; Varner, J. A. Targeting Tumor-Associated Macrophages in Cancer. *Trends Immunol.* **2019**, *40*, 310.
- (14) Wies Mancini, V. S. B.; Pasquini, J. M.; Correale, J. D.; Pasquini, L. A. Microglial modulation through colony-stimulating factor-1 receptor inhibition attenuates demyelination. *Glia* **2019**, *67*, 291.
- (15) Lee, S. H.; Shi, X. Q.; Fan, A.; West, B.; Zhang, J. Targeting macrophage and microglia activation with colony stimulating factor 1 receptor inhibitor is an effective strategy to treat injury-triggered neuropathic pain. *Mol. Pain* **2018**, *14*, 174480691876497.
- (16) Papadopoulos, K. P.; Gluck, L.; Martin, L. P.; Olszanski, A. J.; Tolcher, A. W.; Ngarmchamnanrith, G.; Rasmussen, E.; Amore, B. M.; Nagorsen, D.; Hill, J. S.; Stephenson, J. First-in-human study of AMG 820, a monoclonal anti-colony-stimulating factor 1 receptor antibody, in patients with advanced solid tumors. *Clin. Cancer Res.* **2017**, *23*, 5703.
- (17) Peyraud, F.; Cousin, S.; Italiano, A. CSF-1R Inhibitor Development: Current Clinical Status. *Curr. Oncol. Rep.* **2017**, *1*.
- (18) Travers, M.; Brown, S. M.; Dunworth, M.; Holbert, C. E.; Wiehagen, K. R.; Bachman, K. E.; Foley, J. R.; Stone, M. L.; Baylin, S. B.; Casero, R. A.; Zahnow, C. A. DFMO and 5-azacytidine increase M1 macrophages in the tumor microenvironment of murine ovarian cancer. *Cancer Res.* **2019**, *79*, 3445.
- (19) Azad, A. K.; Rajaram, M. V. S.; Metz, W. L.; Cope, F. O.; Blue, M. S.; Vera, D. R.; Schlesinger, L. S. -Tilmanocept, a New Radiopharmaceutical Tracer for Cancer Sentinel Lymph Nodes, Binds to the Mannose Receptor (CD206). *J. Immunol.* **2015**, *195*, 2019–2029.
- (20) Zhan, X.; Jia, L.; Niu, Y.; Qi, H.; Chen, X.; Zhang, Q.; Zhang, J.; Wang, Y.; Dong, L.; Wang, C. Targeted depletion of tumour-associated macrophages by an alendronate-glucomannan conjugate for cancer immunotherapy. *Biomaterials* **2014**, *35*, 10046–10057.
- (21) Ehlers, S. DC-SIGN and mannose-6-phosphate-6-phosphoglucoamylase Mycobacterium tuberculosis: a deceptive liaison. *Eur. J. Cell Biol.* **2010**, *89*, 95.
- (22) Lasala, F.; Arce, E.; Otero, J. R.; Rojo, J.; Delgado, R. Mannosyl Glycodendritic Structure Inhibits DC-SIGN-Mediated Ebola Virus Infection in cis and in trans. *Antimicrob. Agents Chemother.* **2003**, *47*, 3970.
- (23) Jameson, B.; Baribaud, F.; Pöhlmann, S.; Ghavimi, D.; Mortari, F.; Doms, R. W.; Iwasaki, A. Expression of DC-SIGN by dendritic cells of intestinal and genital mucosae in humans and rhesus macaques. *J. Virol.* **2002**, *76*, 1866–1875.
- (24) Scodeller, P.; Simón-Gracia, L.; Kopanchuk, S.; Tobi, A.; Kilk, K.; Säälil, P.; Kurm, K.; Squadrito, M. L.; Kotamraju, V. R.; Rinken, A.; De Palma, M.; Ruoslahti, E.; Teesalu, T. Precision Targeting of Tumor Macrophages with a CD206 Binding Peptide. *Sci. Rep.* **2017**, *7*, 1.
- (25) Ascitutto, E. K.; Kopanchuk, S.; Lepland, A.; Simón-Gracia, L.; Aleman, C.; Teesalu, T.; Scodeller, P. Phage-Display-Derived Peptide Binds to Human CD206 and Modeling Reveals a New Binding Site on the Receptor. *J. Phys. Chem. B* **2019**, *123*, 1973.
- (26) Scodeller, P.; Ascitutto, E. K. Targeting Tumors Using Peptides. *Molecules* **2020**, *25*, 808.
- (27) Rashid, M. H.; Borin, T. F.; Ara, R.; Alptekin, A.; Liu, Y.; Arbab, A. S. Generation of novel diagnostic and therapeutic exosomes to detect and deplete pro-tumorigenic M2-macrophages. *Adv. Therap.* **2020**, 1900209.
- (28) Bobko, A. A.; Eubank, T. D.; Voorhees, J. L.; Efimova, O. V.; Kirilyuk, I. A.; Petryakov, S.; Trofimov, D. G.; Marsh, C. B.; Zweier, J. L.; Grigor'Ev, I. A.; Samouilov, A.; Khrantsov, V. V. In vivo monitoring of pH, redox status, and glutathione using L-band EPR for assessment of therapeutic effectiveness in solid tumors. *Magn. Reson. Med.* **2012**, *67*, 1827–1836.
- (29) Case, D. A.; Betz, R. M.; Botello-Smith, W.; Cerutti, D. S.; Cheatham, T. E.; Darden, T. A.; Duke, R. E.; Giese, T. J.; Gohlke, H.; Goetz, A. W.; Homeyer, N.; Izadi, S.; Janowski, P.; Kaus, J.; Kovalenko, A.; Lee, T. S. *Amber* **18**, 2018.
- (30) Maier, J. A.; Martinez, C.; Kasavajhala, K.; Wickstrom, L.; Hauser, K. E.; Simmerling, C. ff14SB: Improving the Accuracy of Protein Side Chain and Backbone Parameters from ff99SB. *J. Chem. Theory Comput.* **2015**, *11*, 3696–3713.
- (31) Jorgensen, W. L.; Chandrasekhar, J.; Madura, J. D.; Impey, R. W.; Klein, M. L. Comparison of simple potential functions for simulating liquid water. *J. Chem. Phys.* **1983**, *79*, 926–935.
- (32) Hu, Z.; Shi, X.; Yu, B.; Li, N.; Huang, Y.; He, Y. Structural Insights into the pH-Dependent Conformational Change and Collagen Recognition of the Human Mannose Receptor. *Structure* **2018**, *26*, 60–71.
- (33) Yang, J.; Zhang, Y. I-TASSER server: New development for protein structure and function predictions. *Nucleic Acids Res.* **2015**, *43*, W174.

- (34) Zhang, C.; Freddolino, P. L.; Zhang, Y. COFACTOR: Improved protein function prediction by combining structure, sequence and protein-protein interaction information. *Nucleic Acids Res.* **2017**, *45*, W291.
- (35) Simon-Gracia, L.; Scodeller, P.; Fuentes, S. S.; Vallejo, V. G.; Rios, X.; San Sebastian, E.; Sidorenko, V.; Di Silvio, D.; Suck, M.; De Lorenzi, F.; Rizzo, L. Y.; von Stillfried, S.; Kilk, K.; Lammers, T.; Moya, S. E.; Teesalu, T. Application of polymersomes engineered to target p32 protein for detection of small breast tumors in mice. *Oncotarget* **2018**, *9*, 18682–18697.
- (36) Paasonen, L.; Sharma, S.; Braun, G. B.; Kotamraju, V. R.; Chung, T. D. Y.; She, Z.-G.; Sugahara, K. N.; Yliperttula, M.; Wu, B.; Pellecchia, M.; Ruoslahti, E.; Teesalu, T. New p32/gC1qR Ligands for Targeted Tumor Drug Delivery. *ChemBioChem* **2016**, *17*, 570–575.
- (37) Jaynes, J. M.; Sable, R.; Ronzetti, M.; Bautista, W.; Knotts, Z.; Abisoye-Ogunniyan, A.; Li, D.; Calvo, R.; Dashnyam, M.; Singh, A.; Guerin, T.; White, J.; Ravichandran, S.; Kumar, P.; Talsania, K.; Chen, V.; Ghebremedhin, A.; Karanam, B.; Bin Salam, A.; Amin, R.; Odzorig, T.; Aiken, T.; Nguyen, V.; Bian, Y.; Zarif, J. C.; de Groot, A. E.; Mehta, M.; Fan, L.; Hu, X.; Simeonov, A.; Pate, N.; Abu-Asab, M.; Ferrer, M.; Southall, N.; Ock, C. Y.; Zhao, Y.; Lopez, H.; Kozlov, S.; de Val, N.; Yates, C. C.; Baljinnam, B.; Marugan, J.; Rudloff, U. Mannose receptor (CD206) activation in tumor-associated macrophages enhances adaptive and innate antitumor immune responses. *Sci. Transl. Med.* **2020**, *12*, eaax6337.
- (38) Ueno, N.; Bratt, C. L.; Rodriguez, N. E.; Wilson, M. E. Differences in human macrophage receptor usage, lysosomal fusion kinetics and survival between logarithmic and metacyclic *Leishmania infantum* chagasi promastigotes. *Cell. Microbiol.* **2009**, *11*, 1827.
- (39) Cong, Y.; Wu, S.; Han, J.; Chen, J.; Liu, H.; Sun, Q.; Wu, Y.; Fang, Y. Pharmacokinetics of homoplaginin in rats following intravenous, peritoneal injection and oral administration. *J. Pharm. Biomed. Anal.* **2016**, *129*, 405.
- (40) Bharat, A.; Bhorade, S. M.; Morales-Nebreda, L.; McQuattipimentel, A. C.; Soberanes, S.; Ridge, K.; DeCamp, M. M.; Mestan, K. K.; Perlman, H.; Budinger, G. R. S.; Misharin, A. V. Flow cytometry reveals similarities between lung macrophages in humans and mice. *Am. J. Respir. Cell Mol. Biol.* **2016**, *54*, 147.
- (41) Mann, A. P.; Scodeller, P.; Hussain, S.; Joo, J.; Kwon, E.; Braun, G. B.; Molder, T.; She, Z.-G.; Kotamraju, V. R.; Ranscht, B.; Krajewski, S.; Teesalu, T.; Bhatia, S.; Sailor, M. J.; Ruoslahti, E. A peptide for targeted, systemic delivery of imaging and therapeutic compounds into acute brain injuries. *Nat. Commun.* **2016**, *7*, 1–11.
- (42) Cooney, C. A.; Jousheghany, F.; Yao-Borengasser, A.; Phanavanh, B.; Gomes, T.; Kieber-Emmons, A. M.; Siegel, E. R.; Suva, L. J.; Ferrone, S.; Kieber-Emmons, T.; Monzavi-Karbassi, B. Chondroitin sulfates play a major role in breast cancer metastasis: A role for CSPG4 and CHST11 gene expression in forming surface P-selectin ligands in aggressive breast cancer cells. *Breast Cancer Res.* **2011**, *1*.
- (43) Asparuhova, M. B.; Secondini, C.; Rüegg, C.; Chiquet-Ehrismann, R. Mechanism of irradiation-induced mammary cancer metastasis: A role for SAP-dependent Mkl1 signaling. *Mol. Oncol.* **2015**, *9*, 1510.
- (44) Magnusson, S.; Berg, T. Extremely rapid endocytosis mediated by the mannose receptor of sinusoidal endothelial rat liver cells. *Biochem. J.* **1989**, *257*, 651–656.
- (45) Kim, B.; Sun, S.; Varner, J. A.; Howell, S. B.; Ruoslahti, E.; Sailor, M. J. Securing the Payload, Finding the Cell, and Avoiding the Endosome: Peptide-Targeted, Fusogenic Porous Silicon Nanoparticles for Delivery of siRNA. *Adv. Mater.* **2019**, *31*, 1902952.
- (46) Yan, Z.; Wang, F.; Wen, Z.; Zhan, C.; Feng, L.; Liu, Y.; Wei, X.; Xie, C.; Lu, W. LyP-1-conjugated PEGylated liposomes: A carrier system for targeted therapy of lymphatic metastatic tumor. *J. Controlled Release* **2012**, *157*, 118.
- (47) Laakkonen, P.; Porkka, K.; Hoffman, J. a.; Ruoslahti, E. A tumor-homing peptide with a targeting specificity related to lymphatic vessels. *Nat. Med.* **2002**, *8*, 751–5.
- (48) Luo, G.; Yu, X.; Jin, C.; Yang, F.; Fu, D.; Long, J.; Xu, J.; Zhan, C.; Lu, W. LyP-1-conjugated nanoparticles for targeting drug delivery to lymphatic metastatic tumors. *Int. J. Pharm.* **2010**, *385*, 150.
- (49) Laakkonen, P.; Akerman, M. E.; Biliran, H.; Yang, M.; Ferrer, F.; Karpanen, T.; Hoffman, R. M.; Ruoslahti, E. Antitumor activity of a homing peptide that targets tumor lymphatics and tumor cells. *Proc. Natl. Acad. Sci. U. S. A.* **2004**, *101*, 9381.
- (50) Wang, Z.; Yu, Y.; Ma, J.; Zhang, H.; Zhang, H.; Wang, X.; Wang, J.; Zhang, X.; Zhang, Q. LyP-1 modification to enhance delivery of Artemisinin or fluorescent probe loaded polymeric micelles to highly metastatic tumor and its lymphatics. *Mol. Pharmaceutics* **2012**, *9*, 2646.
- (51) Etzerodt, A.; Tsalkitzi, K.; Maniecki, M.; Damsky, W.; Delfini, M.; Baudoin, E.; Moulin, M.; Bosenberg, M.; Graversen, J. H.; Auphan-Anezin, N.; Moestrup, S. K.; Lawrence, T. Specific targeting of CD163 + TAMs mobilizes inflammatory monocytes and promotes T cell-mediated tumor regression. *J. Exp. Med.* **2019**, *216*, 2394.
- (52) Nywening, T. M.; Wang-Gillam, A.; Sanford, D. E.; Belt, B. A.; Panni, R. Z.; Cusworth, B. M.; Toriola, A. T.; Nieman, R. K.; Worley, L. A.; Yano, M.; Fowler, K. J.; Lockhart, A. C.; Suresh, R.; Tan, B. R.; Lim, K. H.; Fields, R. C.; Strasberg, S. M.; Hawkins, W. G.; DeNardo, D. G.; Goedegebuure, S. P.; Linehan, D. C. Targeting tumour-associated macrophages with CCR2 inhibition in combination with FOLFIRINOX in patients with borderline resectable and locally advanced pancreatic cancer: A single-centre, open-label, dose-finding, non-randomised, phase 1b trial. *Lancet Oncol.* **2016**, *17*, 651.
- (53) Harney, A. S.; Karagiannis, G. S.; Pignatelli, J.; Smith, B. D.; Kadioglu, E.; Wise, S. C.; Hood, M. M.; Kaufman, M. D.; Leary, C. B.; Lu, W. P.; Al-Ani, G.; Chen, X.; Entenberg, D.; Oktay, M. H.; Wang, Y.; Chun, L.; De Palma, M.; Jones, J. G.; Flynn, D. L.; Condeelis, J. S. The selective Tie2 inhibitor rebastinib blocks recruitment and function of Tie2Hi macrophages in breast cancer and pancreatic neuroendocrine tumors. *Mol. Cancer Ther.* **2017**, *16*, 2486.
- (54) Xavier, C.; Blykers, A.; Laoui, D.; Bolli, E.; Vaneyken, I.; Bridoux, J.; Baudhuin, H.; Raes, G.; Everaert, H.; Movahedi, K.; Van Ginderachter, J. A.; Devoogdt, N.; Cavelliers, V.; Lahoutte, T.; Keyaerts, M. Clinical Translation of [68Ga]Ga-NOTA-anti-MMR-sdAb for PET/CT Imaging of Protumorigenic Macrophages. *Mol. Imaging Biol.* **2019**, *21*, 898.
- (55) Discher, D. E.; Ahmed, F. POLYMERSOMES. *Annu. Rev. Biomed. Eng.* **2006**, *8*, 323.
- (56) Simon-Gracia, L.; Hunt, H.; Scodeller, P. D.; Gaitzsch, J.; Braun, G. B.; Willmore, A.-M. A.; Ruoslahti, E.; Battaglia, G.; Teesalu, T. Paclitaxel-Loaded Polymersomes for Enhanced Intraperitoneal Chemotherapy. *Mol. Cancer Ther.* **2016**, *15*, 670.
- (57) Simon-Gracia, L.; Hunt, H.; Scodeller, P.; Gaitzsch, J.; Kotamraju, V. R.; Sugahara, K. N.; Tammik, O.; Ruoslahti, E.; Battaglia, G.; Teesalu, T. iRGD peptide conjugation potentiates intraperitoneal tumor delivery of paclitaxel with polymersomes. *Biomaterials* **2016**, *104*, 247–257.
- (58) Simón-Gracia, L.; Hunt, H.; Teesalu, T. Peritoneal carcinomatosis targeting with tumor homing peptides. *Molecules* **2018**, *23*, 1190.
- (59) Wonder, E.; Simón-Gracia, L.; Scodeller, P.; Majzoub, R. N.; Kotamraju, V. R.; Ewert, K. K.; Teesalu, T.; Safinya, C. R. Competition of charge-mediated and specific binding by peptide-tagged cationic liposome-DNA nanoparticles in vitro and in vivo. *Biomaterials* **2018**, *166*, 52.
- (60) Kang, P. B.; Azad, A. K.; Torrelles, J. B.; Kaufman, T. M.; Beharka, A.; Tibesar, E.; DesJardin, L. E.; Schlesinger, L. S. The human macrophage mannose receptor directs Mycobacterium tuberculosis lipaarabinomannan-mediated phagosome biogenesis. *J. Exp. Med.* **2005**, *202*, 987.
- (61) Madsen, D. H.; Leonard, D.; Masedunskas, A.; Moyer, A.; Jürgensen, H. J.; Peters, D. E.; Amornphimoltham, P.; Selvaraj, A.; Yamada, S. S.; Brenner, D. A.; Burgdorf, S.; Engelholm, L. H.; Behrendt, N.; Holmbeck, K.; Weigert, R.; Bugge, T. H. M2-like macrophages are responsible for collagen degradation through a

mannose receptor-mediated pathway. *J. Cell Biol.* **2013**, *202*, 951–966.

(62) Kole, L.; Das, L.; Das, P. K. Synergistic Effect of Interferon- γ and Mannosylated Liposome-Incorporated Doxorubicin in the Therapy of Experimental Visceral Leishmaniasis. *J. Infect. Dis.* **1999**, *180*, 811.

(63) Liu, L.; Yi, H.; He, H.; Pan, H.; Cai, L.; Ma, Y. Tumor associated macrophage-targeted microRNA delivery with dual-responsive polypeptide nanovectors for anti-cancer therapy. *Bio-materials* **2017**, *134*, 166.

(64) Baer, C.; Squadrito, M. L.; Laoui, D.; Thompson, D.; Hansen, S. K.; Kiiäläinen, A.; Hoves, S.; Ries, C. H.; Ooi, C.-H.; De Palma, M. Suppression of microRNA activity amplifies IFN- γ -induced macrophage activation and promotes anti-tumour immunity. *Nat. Cell Biol.* **2016**, *18*, 790–802.

(65) Rodell, C. B.; Arlauckas, S. P.; Cuccarese, M. F.; Garris, C. S.; Li, R.; Ahmed, M. S.; Kohler, R. H.; Pittet, M. J.; Weissleder, R. TLR7/8-agonist-loaded nanoparticles promote the polarization of tumour-associated macrophages to enhance cancer immunotherapy. *Nat. Biomed. Eng.* **2018**, *2*, 578.

(66) Gao, R. W.; Teraphongphom, N.; de Boer, E.; Berg, N. S. v. d.; Divi, V.; Kaplan, M. J.; Oberhelman, N. J.; Hong, S. S.; Capes, E.; Colevas, A. D.; Warram, J. M.; Rosenthal, E. L. Safety of panitumumab-IRDye800CW and cetuximab-IRDye800CW for fluorescence-guided surgical navigation in head and neck cancers. *Theranostics* **2018**, *8*, 2488.

(67) Mann, A. P.; Scodeller, P.; Hussain, S.; Braun, G. B.; Mölder, T.; Toome, K.; Ambasadhan, R.; Teesalu, T.; Lipton, S. A.; Ruoslahti, E. Identification of a peptide recognizing cerebrovascular changes in mouse models of Alzheimer's disease. *Nat. Commun.* **2017**, *8*, 1–11.

(68) Han, Z.; Zhou, Z.; Shi, X.; Wang, J.; Wu, X.; Sun, D.; Chen, Y.; Zhu, H.; Magi-Galluzzi, C.; Lu, Z. R. EDB fibronectin specific peptide for prostate cancer targeting. *Bioconjugate Chem.* **2015**, *26*, 830.

(69) Altmann, A.; Sauter, M.; Roesch, S.; Mier, W.; Warta, R.; Debus, J.; Dyckhoff, G.; Herold-Mende, C.; Haberkorn, U. Identification of a novel ITG α v β 6-binding peptide using protein separation and phage display. *Clin. Cancer Res.* **2017**, *23*, 4170.